Laser Ablation and Seeding for the Preparation of Highly Transparent Copper Conductive Networks on Glass

Joel N. Schrauben

Electro Scientific Industries, 13900 NW Science Park Drive, Portland, Oregon, USA
E-mail: schraubenj@esi.com

This report describes a novel process for preparing transparent conducting networks of Cu on glass. An ultrafast green laser is utilized to remove material from a transparent glass substrate, and a second laser source deposits Cu droplets through the laser-induced forward transfer of a donor film into the laser-etched features. Electroless plating methods that employ the Cu droplets as seeds for plating are then used to fill in the laser-etched features. The geometry and connections of the features are completely determined by the laser processing parameters, which offers great flexibility for tuning the electrical and optical properties of the transparent conducting electrode. Honeycomb and crosshatched patterns comprising 10 μm wide wires with variable pitch were plated on borosilicate glass substrates. The crosshatched patterns have sheet resistances less than 1 Ω □$^{-1}$ and transmittance over 90% across the visible, surpassing typical ITO performance. Microscopic imperfections were observed in the plated material, which, in addition to shrinking the size of the plated features, represent fruitful space for further optimization of the process.

DOI: 10.2961/jlmn.2019.01.0007
Keywords: electrodes, transparent conductors, metal patterning, laser machining

1. Introduction

Transparent conducting electrodes (TCEs) are used in a variety of electronic applications, including displays, touch screens, solar cells, photodetectors, and anti-fogging devices. The most widely used TCE is ITO (tin-doped indium oxide). The material is typically vacuum sputtered onto a transparent substrate, usually glass, and the popularity of this material arises from ITO thin films having sheet resistances as low as ~ 10 Ω □$^{-1}$ (Ohms per square) and transmittance of over 90%. The price of the material is tied to the price of indium, a relatively scarce element at 0.05 ppm in the Earth's crust, and produced at only about 400 tons/year as of 2007.[1] The scarcity of indium is such that the Royal Society of Chemistry has estimated that the supply of indium may run dry by the end of the century.[2] An additional drawback of this material is that ITO films are brittle and not amendable toward flexible applications. As a result, a number of research groups are currently working on alternative strategies for producing transparent conducting materials that employ earth abundant and flexible materials.

There are several strategies for replacing ITO with more earth abundant materials: micro- and nanowire metallic mesh, notably of Cu or Ag, graphene films, carbon nanotube networks, and conductive polymer films (such as PEDOT:PSS).[3,4] Of these, metal mesh and nanowire films, collectively called conducting networks, present some of the best transmittance and sheet resistance values while offering the lowest process and materials costs.[3] The processes used to make nanowire conducting networks can be divided into template and non-template based processes, with the template-based methods relying on lithography and the non-template methods having random alignment of the constituent moieties, using spin coating, dip coating, or spray coating.[5] For both, as transmittance of light is increased the bulk conductivity behavior is lost as the density of wires and number of connections decreases, and conductivity changes according to a percolation scaling law.[6] Metal nanowire meshes typically employ either Ag or Cu nanowires, both generally offering sheet resistances of < 100 Ω □$^{-1}$, and these materials can be used with flexible substrates (see for example: [7–11]). Cu is approximately 100-fold less expensive than Ag, and 1000-fold more abundant, making Cu meshes a much more interesting target for large-scale processes. However, nanostructures of Ag do not oxidize appreciably under ambient conditions and Cu nanostructures do; this has led to some novel work on coating Cu nanowires to mitigate oxidative damage (for example:[12,13]).

Methods for patterning micro-scale metal meshes generally employ nanoparticle inks (typically Ag) which are screen printed or used to fill stamped features.[14] For these, the width of the printed features must be below ~10 μm so that they remain invisible to the naked eye.

Laser-based methods have been employed for preparing transparent conducting networks. Spechler and Arnold demonstrated substantial reduction in surface resistance of a Ag nanowire network on glass following laser processing at low fluence with high exposure time (*ca.* 30 μs) with excitation near the plasmonic resonance of the wires.[15] A laser direct writing approach was employed by Paeng *et al.* for the fabrication of thin Cu transparent conductors.[16] Selective laser ablation of a thin Cu film mounted on glass or flexible substrates was carried out, leaving a wire mesh network with 83% transmittance and sheet resistance of about 17 Ω □$^{-1}$. Lee *et al.* prepared Ni networks through the laser-based reductive sintering of NiO nanoparticles to prepare ~40 nm deep wires of Ni that are *ca.* 10 μm wide.[17] The transmittance of the pattern is controlled by modifying the pitch of the deposited features.

In this report, a novel method is described for the preparation of transparent conducting networks on glass substrates. The method, deemed laser seeding, has been described previously for the preparation of multilayer printed circuit boards on glass dielectrics.[18–20] In the laser seeding process, laser ablation is carried out to prepare the desired features on a dielectric substrate, and the recessed features are seeded with Cu droplets through the laser-induced forward transfer (LIFT) of a Cu foil **(Figure 1)**. While generally the droplets are too sparse to prepare a conductive pattern, they can be utilized as seeds for the deposition of Cu through electroless deposition methods.[21]

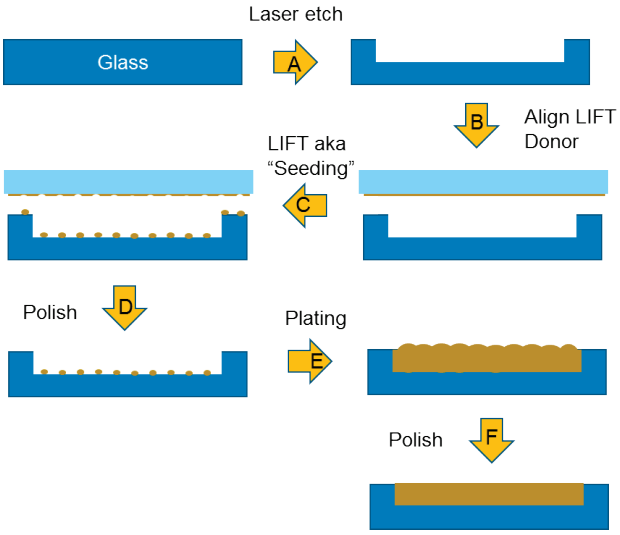

Fig. 1. The laser seeding process. **A.** In the first step, features are machined into a substrate through laser ablation. **B-C**. These features are then seeded with Cu droplets through the laser-induced forward transfer of a Cu foil. **D.** Excess transferred material outside of the recessed features is removed in a polishing step. **E.** The deposited droplets in the recessed features act as sites for the electroless plating of Cu. **F.** After plating, excess plated material can be removed in a polishing step.

In LIFT a laser is focused onto a donor material that is bound to a transparent supporting substrate. The heating of the donor material results in the ejection and transfer of the material to a receiving substrate. Other LIFT methods can be found that utilize sacrificial layers that work to propel the donor material. The first application of the LIFT technique toward the printing of conductive materials was described in 1986 by Bohandy *et al*. for the deposition of Cu onto silicon substrates.[22] Since then, the technique has been applied to deposit a variety of materials onto many different substrates, including the transfer of organic and biological materials.[23–25] A recent active area in LIFT research is the printing of conductive inks and nanopastes,[26] which offer the promise of a high degree of shape and size control for the deposited material. However, the inks themselves generally have conductivities several orders of magnitude less than their bulk counterparts, some of which can be mitigated through *in situ* laser curing or sintering of the deposited ink.[27]

In addition to a high level of interest in LIFT of conductive nanopastes, there has also recently been a surge in interest in LIFT of solid Cu donor films. Conventional approaches for the LIFT of solid Cu donors typically utilize Cu films around 200 nm thick (see, for example [28–30]). Recently, several groups have begun to use Cu donor films with 0.5–1 μm thickness, to print larger features. Of note, Li *et al*. employ a two laser methodology to create stabile nozzle-free jetting of molten Cu from donor films up to 620 nm thick to prepare 1.5 μm diameter droplets.[31] In their method, a 1064 nm QCW laser with a large focused spot is utilized to locally heat the donor film, and a picosecond laser pulse at 355 nm initiates the jet from the melt pool. Kotler and coworkers employ solid Cu films up to 1 μm thick to print structures consisting of voxels of Cu with ~5 μm diameter through a LIFT mechanism that they call a "thermally-induced nozzle," allowing for high stability and directionality of printing.[32–34] The donor films utilized in this report are significantly thicker, ~5 μm thick, than those typically used for the LIFT of solid Cu.

2. Experimental methods

Glass etching/ablation was carried out on an ESI Lodestone system, utilizing an Eolite Chinook green laser, operating at 515 nm, *ca.* 800 fs pulse duration, and 1 MHz pulse repetition frequency. The parameters for each design are listed in the main text of the report. Glass substrates used in this work are 1 mm thick borosilicate microscope slides from Corning, cleaned by rinsing with methanol and wiped dry using a lens wipe, and handled only with gloved hands.

In the LIFT process a laser is focused onto a Cu foil that is adhered to a glass substrate, which is referred to as the "donor" substrate. To prepare the donor substrate, a 4% aqueous solution of poly(vinyl alcohol) (PVA) is spin coated onto a 1 mm thick borosilicate glass slide and the film allowed to dry for several hours to produce a uniform coating about 1 μm thick. The Cu foil, as received from Oak-Mitsui, consists of a *ca.* 5 μm thick Cu foil bound to a 35 μm carrier layer of Cu. The thin foil is laminated onto the PVA layer using a hot press operating near the melting point of PVA for several minutes. For this, the 5 μm Cu layer was placed in contact with the PVA layer, and the carrier side is facing out. After lamination, the carrier layer can be easily peeled away leaving the thin layer adhered to the glass supporting substrate. The carrier layer is removed just prior to carrying out forward transfer.

An ESI 5335 micromachining platform was utilized for Cu forward transfer. The system utilizes a third-harmonic Nd:YAG laser (355 nm) with pulse repetition frequencies up to 90 kHz, pulse duration ~95 ns, ~12 μm focused beam diameter, and maximum average power of around 11 W. Sufficiently large bite sizes (beam distance travelled in between pulses) to minimize damage to the receiving substrate and sufficiently low pulse energies to maintain good resolution of the deposited Cu must be used for the process. Typical parameters are 40 kHz, 1–1.5 W average power, and bite size 10 μm. The donor material is placed in contact with the receiver, *i.e.*, no additional donor-receiver gap is imposed. This approach leads to deposited Cu features that are several times wider than the ablated trenches. The excess material is removed through gentle mechanical polishing of the substrate surface, leaving Cu droplets only in the ablated features.

Electroless Cu plating was carried out after seeding using standard recipes.[21] A typical recipe utilizes distilled water as the solvent, copper(II) sulfate pentahydrate as the Cu source, potassium sodium tartrate as a chelator, and formaldehyde as a reductant. The pH of the aqueous solution is raised with sodium hydroxide to tune the reduction potentials to drive the plating reaction. The plating was carried out at room temperature in a 200 ml pyrex beaker with magnetic stirring at 200 rpm. The Cu is allowed to overgrow the laser etched feature, and after plating the excess material is mechanically removed using a piece of very fine grit sand paper (600 grit or greater).

Profile and height map measurements of the laser ablated features were carried out on a Keyence VK9700 scanning laser microscope. Profiles of the features were analyzed using the VK Analysis Application, version 3.1.0.0. Resistance measurements of the transparent touch pad designs used a digital multimeter. A large variation in the measured closed circuit configuration was found, based on the geometry of the fingertip, pressure applied and other factors, and the values given in the main body of this report are representative values. Four point probe Van der Pauw measurements of the wire mesh features employed an Agilent E3612A DC power supply for establishing currents from 50-200 mA across the plated pattern, and a digital multimeter was used for recording the voltage drop. The reported resistivity values are the average of 4 measurements at different applied currents for each plated feature. Optical transmittance measurements were carried out using an Ocean Optics Flame-S spectrometer with data acquisition through the Oceanview spectroscopy software program, version 1.5.2. An Ocean Optics LS-1 tungsten halogen light source was utilized for these measurements. The transmittance spectrum of a blank 1 mm thick borosilicate glass slide was used as a reference spectrum. Reflective losses from both surfaces of the blank glass slide result in a measured transmittance of *ca.* 93% across the visible range.

3. Wire meshes on glass substrates.

LIFT is used in the process outlined in Figure 1 to prepare a seed layer of Cu particles bound to the glass receiving substrate. These Cu particles are locations for electroless plating and, to ensure uniform plating, the Cu particles must be uniformly distributed in the recessed feature. For seeding the plating of the wire mesh patterns that constituent the conductive elements of the transparent conducting electrodes prepared in this report, a pulse energy was chosen below the damage threshold for the glass receiving substrate (about 50 μJ), but above the regime observed around 25 μJ/pulse, where only single large droplets of Cu are deposited. (The formation and application of these large Cu voxels is an intriguing topic beyond the scope of this work, and is discussed in a forthcoming report.[35]) To avoid damage to both the deposited Cu features and the glass receiver, a bite (pulse-to-pulse spacing) comparable to the focused laser beam diameter was chosen. **Figure 2A** shows one example of a seeded pattern prior to plating utilizing laser processing parameters of 355 nm emission wavelength, 40 kHz, 1.5 W (37.5 μJ/pulse) and beam velocity of 400 mm/s (10 μm bite). The deposited Cu is uniform in composition and is much wider than the *ca.* 10 μm wide recessed features of the laser-ablated pattern. Gentle polishing is used to remove the excess Cu from the glass substrate, leaving Cu only in the desired areas, *i.e.*, the recessed features prepared by laser ablation (Figure 2A, right). Electroless Cu plating is then carried out using standard methods[21] using the laser-deposited Cu droplets as seeds for the autocatalytic immersion plating process. After plating, a second polish step can be employed to remove any excess material outside of the recessed features of the mesh pattern.

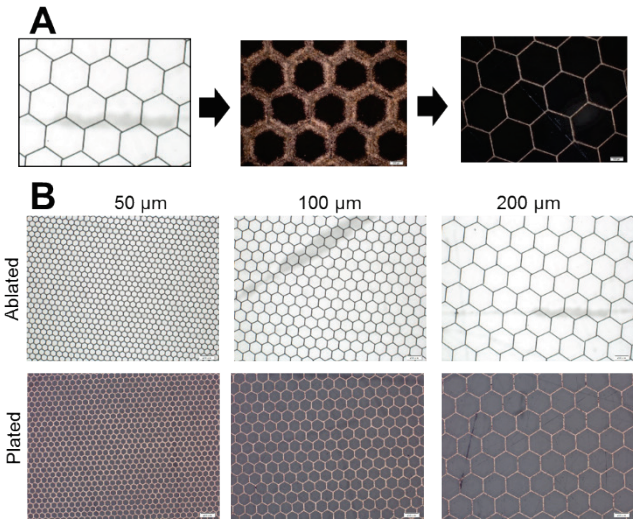

Fig. 2. A. Process flow prior to plating. **Left:** Trenches prepared in the borosilicate glass substrate by sub-picosecond laser ablation. **Middle**: Dark field micrograph of a seeded wire mesh pattern. The processing parameters are 40 kHz, 1.5 W (37.5 μJ/pulse) and 400 mm/s (10 μm bite). **Right:** The same pattern is shown after polishing off the excess Cu, leaving Cu only in the recessed features. The scale bar in these micrographs is 100 μm. **B.** Micrographs of the honeycomb patterns after laser ablation of the glass substrate and after seeding by LIFT and plating in an electroless plating bath. The scale bar in these micrographs is 200 μm

Initial designs employed a honeycomb shape (Figure 2 and **Figure S1**) with the side of the constituent hexagons 50, 100, or 200 μm long. Patterning of the borosilicate glass substrate by laser ablation was carried out with a 515 nm laser with ~ 800 fs pulse duration operating at 1 MHz pulse repetition frequency, 3 μJ/pulse and beam velocity of 1000 mm/s. The pattern was repeated with n = 1, 2 or 3 times to produce trenches with depth of 1.05 ± 0.28 μm, 4.83 ± 0.78 μm, and 6.95 ± 0.21 μm (± 1σ), respectively, with width around 10 μm (Supporting Information, **Table S1**). The depth increases with the number of repetitions of the pattern, while the width of the features remains unchanged at around 10 μm. As expected for laser processing in this pulse duration regime, no heat affected zone or recast is apparent on the patterns. The designs are 10 x 20 mm. Based on the lack of transmittance of the plated material (Cu) across the visible, the expected transmittance of the design can be estimated as the fraction of the glass surface for the pattern, *i.e.*, the non-plated fraction of the surface. To measure this, height maps of the laser-ablated patterns were generated through UV scanning laser microscopy. The unrecessed area of the non-plated, laser-ablated patterns was measured and is reported

as the non-plated area in **Table 1**. For the 50 μm honeycomb pattern repeated 3 times, 81% of the surface area is unrecessed; this value increases to 89% for the 100 μm pattern and 94% for the 200 μm pattern.

Transmittance measurements at 500 nm of the honeycomb meshes are also presented in Table 1. The transmittance spectra are presented in **Figure 3** for hexagon edge lengths of 50, 100 and 200 μm when the laser machining pattern is carried out 3 times. At 500 nm the transmittance of the 200 μm pattern is around 90%, 82% for the 100 μm pattern, and 67% for the 50 μm pattern. The transmittance values across *n* do not vary within the error of the measurements, consistent with the width measurements of the laser ablated features. The reported transmittance values vary from the measurements of the non-plated area (Table 1). These differences can be explained by over-plating of the sample and microscopic scratches from the post-plating polishing step, both of which adversely affect the final transmittance of the sample.

Table 1. Measured non-ablated area and transmittance (*T*) at 500 nm for each honeycomb mesh sample with repetitions *n*.

Hexagon Edge [μm]	*n*	Non-plated area [%]	*T* at 500 nm [%]
50	1	85.8	68.0
50	2	82.2	69.3
50	3	81.0	67.2
100	1	93.0	86.1
100	2	90.5	83.3
100	3	89.1	82.9
200	1	95.3	93.1
200	2	94.3	90.3
200	3	94.2	91.5

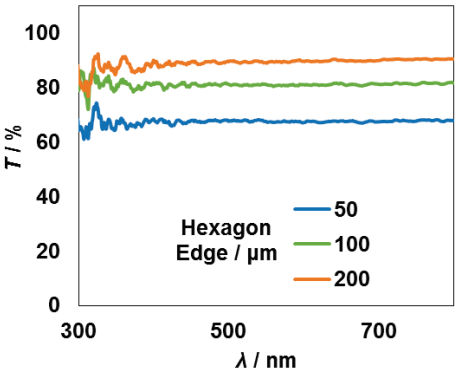

Fig. 3. Transmittance measurements of hexagon patterns with three repetitions of the laser machining pattern.

To determine the sheet resistance of the conductive meshes, square mesh designs were made in the borosilicate glass substrate. Designs used a line-to-line spacing (pitch) of 200, 300, or 400 μm and covered a total area of 20x20 mm (**Figure S2** shows drawings of these designs). In machining the design, a row of trenches is made in the material through laser ablation, and then the perpendicular trenches are made. The design includes pads at the corners of the mesh pattern, which are used for determining the sheet resistance of the pattern. The pads utilize a 7 μm pitch crosshatch pattern for preparing a recessed feature with dimensions of 1 mm^2. For patterning on glass the wires and pads were made using a laser at 515 nm, ~ 800 fs pulse duration, 2.5 W, 1 MHz, 1500 mm/s beam velocity, and 5 repetitions of the pattern.

A second pattern with a "touchpad" design consisting of interdigitated wires that connect on each end to a common collector and pad was also prepared (Figure S2, Bottom). Touching the interdigitated wires of the pattern provides a means for current to flow from one set of wires to the other. Designs were prepared with 200 μm and 400 μm pitch between the wires. The design in borosilicate glass was carried out with the same laser processing parameters described above for the wire mesh pattern. The collection bar at the end, wire leading to the pad, and pad were made using these parameters with a 7 μm pitch crosshatch pattern.

Profile measurements of the ablated features indicate that the channels made in the glass are approximately 10 μm wide and 5-6 μm deep, and when wires intersect the depth is slightly more than double this amount (**Figure S3**). The photos presented in **Figure 4** show the plated crosshatched wire patterns in panels A-B and the plated touchpad patterns in C-D in both normal and tilted orientations.

Figures 4 E-F show optical micrographs of the plated touchpad and mesh patterns with 200 μm pitch. The pictures show that there are many inhomogeneities in the wires—voids and gaps—that may be the result of poor plating, misalignment in the seeding process, or overly aggressive polishing in the post-processing steps. These will undoubtedly affect the electrical characteristics of the features, and represent a clear opportunity for optimizing the process conditions. Figures 4 G-H show cross section micrographs of the wires in the 200 μm pitch touch pad design, which confirm that the wires are the same dimensions as the laser ablated trenches and are composed of bulk Cu from electroless plating. Furthermore, the plated features have relatively smooth surfaces, an important characteristic for high frequency electronic applications.

As with the honeycomb patterns discussed above, the geometry of the ablated features can be used to estimate the fraction of transmitted light that one would expect in the plated design. From the measured 10 μm wire width, ~ 5% and ~2.5% of the surface area is estimated to be plated for the 200 μm and 400 μm pitch touchpad patterns, respectively, leading to estimates of 95% and 97.5% transmittance. Measurements corrected for the transmittance of the glass slide show a transmittance greater than 92% and 95%, respectively, across the visible for these two plated patterns. The wire mesh patterns have approximately twice the density of wires for the same pitch as the touchpad patterns, so estimates of 90% and 95% transmittance are made for 200 μm and 400 μm wire mesh patterns, and measurements of >89% and >93% were made. As with the honeycomb patterns described above, the lower measured transmittance compared to the estimated value is ascribed to over-plating the feature and/or microscopic scratches on the glass from the polishing step (which can be observed in Figure 4 E-F), both of which would lower the transmittance.

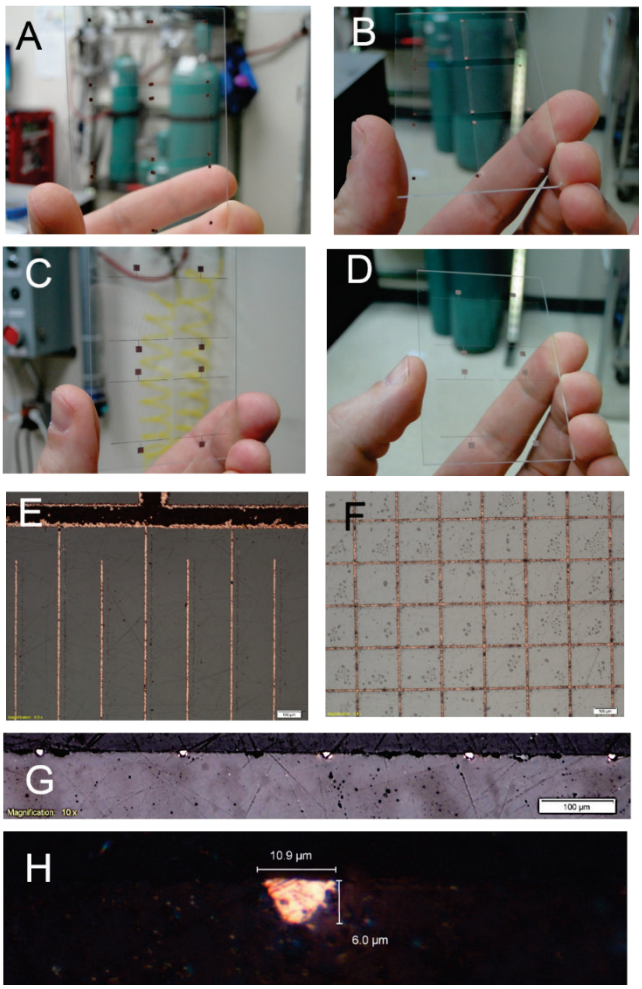

Fig. 4. Photographs and micrographs of the plated designs. **A-B.** Photos of the wire mesh design. The design is printed on both the front and back sides of the glass piece, with pad features overlapping somewhat in the middle. **C-D.** Touch pad design. Two copies of each pattern are printed side-by-side on one 50x75x1 mm^3 piece of glass. **E-F.** 10x magnification optical micrographs of the touchpad and mesh patterns with 200 µm pitch showing microscopic imperfections in the wires and on the glass surface. The scale bar is 100 µm. **G-H.** Cross section micrographs of the wires at 10x and 50x magnification from the 200 µm pitch touchpad design.

Clearly, the application of thinner wires would be advantageous toward increasing the transmittance, and would allow for a higher number of wire-wire connections while maintaining a high transmittance. Efforts were made to prepare thinner wires for both patterns in glass by lowering the pulse energy and increasing the beam velocity, and in doing so features with widths as thin as 3 µm were prepared, but the result across the entire 20x20 mm pattern was inconsistent. Modifying the optics path of the beam to include a faster focus optic for tighter focusing will be necessary to obtain the necessary damage threshold energy for consistent machining over smaller areas.

Simple electrical characterization was carried out for these patterns. For the wire mesh patterns, measurements of the sheet resistance were carried out using the Van der Pauw method. In this method four contacts are placed on the corners of the sample, and current is applied along one of the edges of the pattern through two adjacent pads while the voltage drop is measured across the other two pads. Application of Ohm's law yields a resistance value unique to that configuration. If the placement of the contacts and the sample itself are both symmetric, then the calculated sheet resistance R_s should be invariant with the placement of the contacts, and R_s is given by Equation (1).

$$R_s = \pi R / \ln(2) \quad (1)$$

Four currents were applied to each wire mesh sample ranging from 20-150 mA and the voltage drop recorded. Sheet resistances of 0.499 ± 0.016 Ω □$^{-1}$ and 0.995± 0.007 Ω □$^{-1}$ (±1σ) were measured for 200 µm and 300 µm pitch patterns respectively (**Table 2**). For the 400 µm pitch pattern, an initial measurement of 0.361± 0.005 Ω □$^{-1}$ was made, and after re-positioning the contacts a sheet resistance of 0.767±0.010 Ω □$^{-1}$ was measured. The reported errors in these four measurements is < 5%, which only confirms that Ohm's law applies to these meshes. Much larger errors are observed when the contacts are repositioned, as is the case for the 400 µm pitch pattern. In all cases the sheet resistance values are measured to be < 1 Ω □$^{-1}$. One would expect a lower sheet resistance for the higher density meshes, *i.e.*, those with lower pitch, but this is not observed, likely because the actual error in the measurement is on the order of the measurement itself, approximately 0.5 Ω □$^{-1}$. This can arise from experimental errors, for example poor soldering to the pads, or from inhomogeneities in the Cu seeding and plating process such as those observed in Figure 4.

Table 2. Sheet resistance of the square wire mesh design.

Pitch [µm]	Ω □$^{-1}$
200	0.499± 0.016
300	0.995± 0.007
400	0.361± 0.005
400	0.767±0.010

Table 3. Operation of touchpad design on glass.

Pitch [µm]	ID	Open [GΩ]	Closed[a] [kΩ]
200	1	0.735	47
200	2	>2	180
400	1	>2	205
400	2	>2	730

[a)]index finger lightly pushing in center of pad

For the touchpad design a digital multimeter was used to measure the resistance in the open and closed configurations in two of the 200 µm pitch patterns and two of 400 µm pitch patterns. In three out of the four patterns the open resistance was larger than the multimeter could measure (>2 GΩ); the exception was one of the 200 µm pitch patterns, where an open resistance of 0.735 GΩ was recorded (**Table 3**). The closed configuration, with a fingertip lightly pushing in the center of the pad, yielded values of 47 kΩ and 180 kΩ for the 200 µm pitch patterns and 205 kΩ and 730 kΩ for the 400 µm pitch patterns, representing a change in resistance of a factor of 10^3 – 10^4 from the open circuit. As with the wire mesh pattern, the difference in the resistance measurements

between samples is quite large, and likely results from inhomogeneities in the laser seeding and plating process that leave microscopic gaps in the wires. Smaller closed resistances are expected for the smaller pitch pattern, and this is roughly observed.

4. Discussion

Ablation of the glass substrate to prepare recessed features for the wire meshes used a laser with 515 nm emission and pulses of *ca.* 800 fs duration. As described by Mourou and coworkers,[36] in this shorter pulse regime, the plasma generated through the laser-material interaction remains localized, which provides the precise machining control and lack of heat-affected zone that is realize in this application. The glass can be patterned at beam velocities up to 2 m/s at the pulse energies used here, allowing for rapid machining of the glass substrates. Glass ablation and modification by ultrashort laser pulses has been documented for several decades, notably in the preparation of microfluidic devices and waveguides (see, for example [37,38] and references therein). Relevant to the work presented here, recent work by Berg *et al.* also demonstrated fine patterning of borosilicate glass with sub-picosecond pulses, into which they print Cu through a LIFT process.[33] They note two regimes of material removal: a cold ablation regime slightly above the ablation threshold that yields rougher surfaces, and a second regime at higher pulse energies wherein glass melting and reflow results in smoother surfaces.

For preparation of the wire meshes, LIFT was carried out at 40 kHz pulse repetition frequency with a beam velocity of 400 mm/s, resulting in a spot-to-spot offset (bite) of 10 μm. Figures 5 and 6 show results from a simulation of 4 pulses closely resembling the experimental conditions (30 μJ/pulse, 40 kHz, 10 μm bite). The simulation models the interaction of laser pulses with the donor substrate, the subsequent melting and ejection of the donor across the air gap between the donor and receiver, and the deposition of this material onto the receiving substrate. The simulations in this work are carried out using a parallel multiphase solver designed to simulate industrial nanosecond laser applications such as laser cutting, drilling, and scribing.[39,40] Specifically, the simulation model considers the propagation and the interaction of the laser beam with the work piece, namely, absorption, reflection, and transmittance. Coupled heat transfer and Navier–Stokes equations are solved to account for the convective and conductive heat transfer during laser processing. Phase transformations (melting, evaporation, re-solidification and condensation) are explicitly modeled during the simulation. In addition, automatic adaptive timestep control and adaptive remeshing techniques are adopted for efficient simulation throughput. Further details of the simulation model can be found in references [41,42], and the material and optical properties used in the simulations are taken from reference [43].

A 100x150 μm^2 (width x length) stack of materials with properties tailored specifically to the laser wavelength of 355 nm was modeled. These materials are: 25 μm of amorphous glass as the supporting substrate, 1 μm of epoxy to simulate the adhesive, 5 μm of Cu donor film, 10 μm of air, and a glass receiving substrate 5 μm thick. Laser processing parameters similar to those of the experiment were chosen, namely, $M^2 = 1.1$, Gaussian beam profile and temporal shape, 355 nm wavelength, 12 μm focused beam diameter at the top of the work surface, 95 ns pulse width and 30 μJ/pulse.

The panels on the left side of Figure 5 show the locations of liquid (orange) and solid (green) Cu 250 ns after the laser pulse arrives at the Cu/glass interface for 1, 2, 3 and 4 pulses. The right side panels in the Figure show a top-down view of the solid Cu deposits resulting from 1-4 pulses. These plots use a logarithmic scale from 10^{-3}–1 to indicate the fractional composition of the mesh element (χ_m). Figure 6 shows the pressure and temperature 250 ns after the laser pulse arrives at the Cu/glass interface for 1, 2, 3 and 4 pulses. In the pressure plots (left side of Figure 6), the solid and liquid components are represented in white, while the pressure of the vapor components, in Pascals, is presented on a logarithmic scale from 10^5-10^8 Pascals. The temperature plots (right side of Figure 6) show the temperature of only the liquid and solid components, using a logarithmic scale from 290-4000 K.

In comparing the ejection of molten Cu produced by the first and subsequent pulses (Figure 5, left panels) it is clear that there is a very different pattern of material ejection for the first laser pulse compared to subsequent laser pulses. At 250 ns, the first pulse results in the ejection of molten Cu in a cone shape, which splashes down onto the receiving substrate symmetrically. After the initial LIFT event from the donor, subsequent laser pulses that fall adjacent to the initial ejection site create molten Cu that is not contained by a nozzle-like feature, but rather is free to eject in the absence of large pressure build up from the donor film through the earlier damage sites. The pressure plots of Figure 6 show much greater pressure, ~10^8 Pascals at 250 ns after the first pulse, than is calculated for subsequent pulses, with maximum pressures of *ca.* 5×10^7 Pascals. For these subsequent pulses, the bulk of the material ejects in a cone along the path of the laser pulse, but a large fraction splashes out from the opening in the donor film produced by the previous LIFT events. As a result, the deposits for each subsequent pulse are asymmetric, composed of two lobes, and are narrower and deeper than what is observed for the first pulse.

While bulk resistivity measurements of the individual wires were not carried out, a previous study utilizing the laser seeding methodology used in the report demonstrated bulk resistivity values of 1–1.5 times the bulk Cu value of 1.68×10^{-8} Ωm.[19] This result represents a significant enhancement in conductivity relative to features that are plated solely by LIFT. For example, Winter and coworkers explored the bulk resistivity of large rectangular structures composed of ~5 μm Cu droplets deposited by LIFT from a 500 nm thick donor film, and found resistivity values 4–14 times the bulk value.[34] They attribute the large resistivity values primarily to scattering from grain boundaries of the nano-sized crystalline structures that are deposited, and also to voids that are present in the printed structure. The same plating process was utilize to prepare recessed conductive Cu structures (lines ~14 μm wide) in borosilicate glass, with reported bulk resistivity 5x that of bulk Cu.[33] It can be inferred that the hybrid LIFT/chemical plating process utilized in this report minimizes grain boundaries and voids through

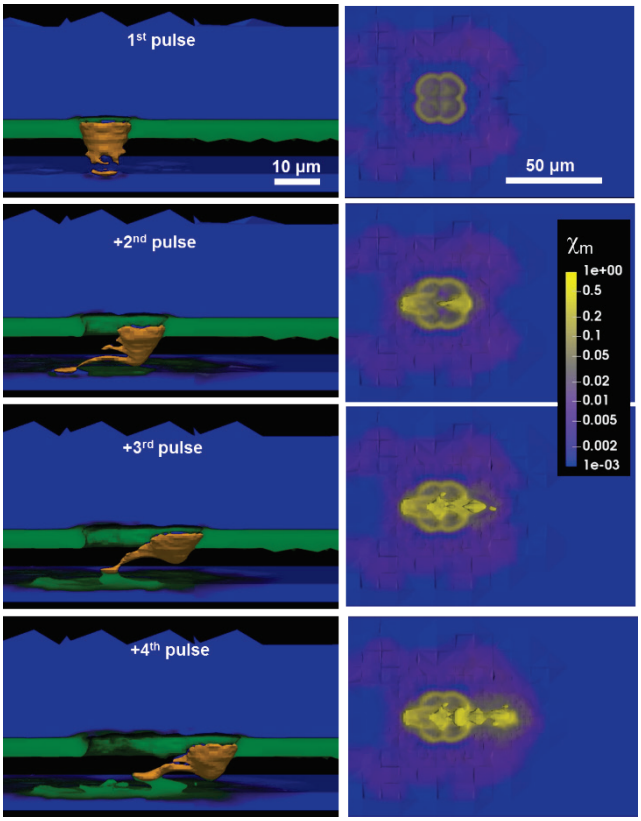

Fig. 5. Simulation of Cu melt flow and deposits resulting from 4 pulses (355 nm, 95 ns, 30 µJ/pulse, 12 µm diameter spot size) with 10 µm bite. **Left:** Cu melt 250 ns after the pulse arrives at the Cu/glass interface for 1, 2, 3 and 4 pulses. Liquid Cu is orange, solid Cu is green, glass is blue and air is black. **Right:** Top-down view of the solid Cu deposits resulting from 1-4 pulses. These plots use a logarithmic scale from 10^{-3}–1 to indicate the fractional composition of the mesh element (χ_m), yellow representing that the mesh element is fully composed of Cu and blue indicating that the mesh element is fully composed of glass.

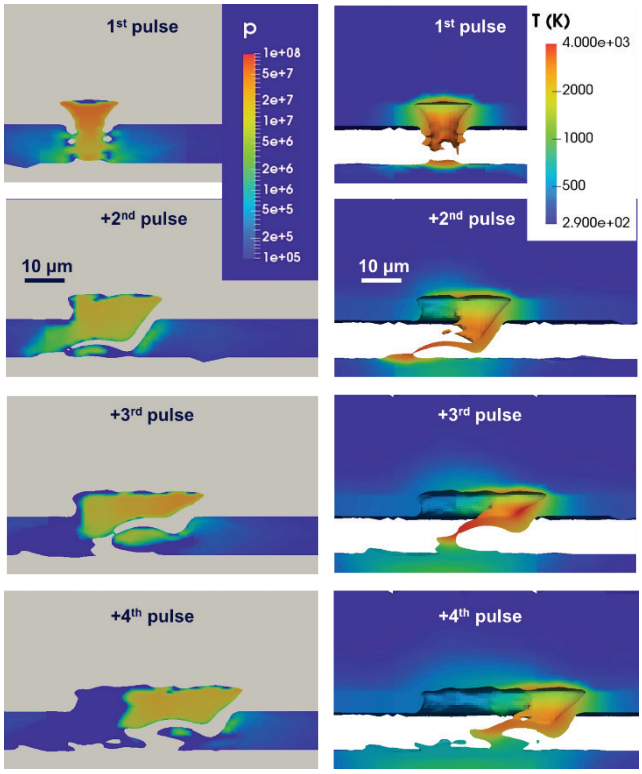

Fig. 6. Simulation of Cu melt flow and deposits resulting from 4 pulses (355 nm, 95 ns, 30 µJ/pulse, 12 µm diameter spot size) with 10 µm bite. **Left:** The pressure in Pascals at 250 ns after the pulse arrives at the Cu/glass interface for 1, 2, 3 and 4 pulses. The pressure scale is logarithmic from 10^5–10^8 Pascals. Solid and liquid components are colored white. **Right:** This column shows the temperature at 250 ns after the pulse arrives at the Cu/glass interface for 1, 2, 3 and 4 pulses. The temperature scale is logarithmic from 290–4000 K. Only solid and liquid components are represented.

the application of chemical plating methods, which are long-established and widely utilized.

The conductive features prepared in this report are much larger than the nanowires typically used in Cu nanowire-based TCEs. However, the dimensions we report, *i.e.*, wires ~10 µm wide, are comparable to those of conductive features prepared by other laser direct-write methodologies, albeit much thicker. For example, Lee et al. used laser direct writing to photosinter NiO-based inks on glass substrates. This technique resulted in 5–10 µm wide Ni wires that were 25–50 nm thick.[17] Another report details ablation of *ca.* 20 nm Cu films on flexible polymer substrates,[16] and the remaining conductive features are 2–10 µm wide. Finally, a number of commercial processes are in development that utilize stamping, molding, or screen printing to prepare cross-hatched metal mesh networks with wire dimensions in the range of 3–25 µm.[14]

The described process offers a number of advantages over current efforts to prepare next-generation transparent conducting materials. Higher conductivities and optical transmittance are found compared to nanowire methods, all while avoiding the synthetic chemistry, wet processing steps, and sintering associated with these methods. Furthermore, concerns regarding oxidation of Cu nanowires are eliminated. The process has very low materials cost compared to ITO or Ag-based methods (*i.e.,* Ag nanowire films or nanoparticle pastes). Finally, there are no special environmental conditions required, such as high vacuum deposition, inert gases, *etc.*, associated with thin-film deposition methods.

5. Conclusions

A technique utilizing two different lasers to plate fine wire meshes on glass for the preparation of transparent conducting electrodes has been demonstrated. A sub-picosecond green laser is applied to ablate a glass substrate in the desired pattern, and these patterns are seeded using a 355 nm, ~95 ns laser to transfer Cu into these features using a LIFT process that utilizes a thick donor substrate. Cu can then be plated on the seeds using standard electroless plating techniques. The Cu meshes on glass provide >90% transmittance with sheet resistances of <1 Ω □$^{-1}$, which approaches or improves upon the state of the art. There remains substantial room for optimization in the process through further narrowing of the wires and improving the LIFT and plating techniques that are used. Future work will focus on these improvements as well as applying the process to soft, flexible and stretchable dielectric materials, and producing functional demonstrators.

Supporting Information
Supporting Information, including additional micrographs of the laser etched and plated honeycomb patterns, is available at http://www.jlps.gr.jp/jlmn/index.php.

Acknowledgements
The author would like to thank Zhibin Lin for assistance and guidance with the simulations, and Jan Kleinert and Chris Ryder for useful discussions that lead to the development of the laser seeding methodology.

References
[1] G. Phipps, C. Mikolajczak and T. Guckes: 22nd EU PV Sol. Conf., Milan, (2007), p. Paper 3BV.5.20.
[2] E. Davies: Chem. World, January, (2011) 50.
[3] G. U. Kulkarni, S. Kiruthika, R. Gupta and K. Rao: Curr. Opin. Chem. Eng., 8, (2015) 60.
[4] K. Ellmer: Nat. Photonics, 6, (2012) 809.
[5] J. Song and H. Zeng: Angew. Chem. Int. Ed., 54, (2015) 9760.
[6] S. De, T. M. Higgins, P. E. Lyons, E. M. Doherty, P. N. Nirmalraj, W. J. Blau, J. J. Boland and J. N. Coleman: ACS Nano, 3, (2009) 1767.
[7] F. Xu and Y. Zhu: Adv. Mater., 24, (2012) 5117.
[8] T. Akter and W. S. Kim: ACS Appl. Mater. Interfaces, 4, (2012) 1855.
[9] H. Lee, K. Lee, J. T. Park, W. C. Kim and H. Lee: Adv. Funct. Mater., 24, (2014) 3276.
[10] S. Li, Y. Chen, L. Huang andD. Pan: Inorg. Chem., 53, (2014) 4440.
[11] W. Hu, R. Wang, Y. Lu andQ. Pei: J. Mater. Chem. C, 2, (2014) 1298.
[12] A. R. Rathmell, M. Nguyen, M. Chi and B. J. Wiley: Nano Lett., 12, (2012) 3193.
[13] Z. Chen, S. Ye, I. E. Stewart andB. J. Wiley: ACS Nano, 8, (2014) 9673.
[14] K. Ghaffarzadeh: "Transparent Conductive Films (TCFs): Emerging Technology and Market Frontiers" (IDTechX Webinar, 2017).
[15] J. A. Spechler and C. B. Arnold: Appl. Phys. A, 108, (2012) 25.
[16] D. Paeng, J.-H. Yoo, J. Yeo, D. Lee, E. Kim, S. H. Ko and C. P. Grigoropoulos: Adv. Mater., 27, (2015) 2762.
[17] D. Lee, D. Paeng, H. K. Park and C. P. Grigoropoulos: ACS Nano, 8, (2014) 9807.
[18] J. Schrauben, C. Tribe, C. Ryder and J. Kleinert: IPC Apex, San Diego, (2017) p.1027.
[19] J. Schrauben, C. Tribe, C. Ryder and J. Kleinert: PCB Mag., August, (2017) 44.
[20] J. Schrauben and J. Kleinert: U.S. Provisional Patent Application E253:P1 (2017).
[21] R. S. Khandpur, Printed Circuit Boards, McGraw-Hill, San Francisco, 2006.
[22] J. Bohandy, B. F. Kim and F. J. Adrian: J. Appl. Phys., 60, (1986) 1538.
[23] M. Nagel and T. Lippert: "Nanomaterials: Processing and Characterization with Lasers" ed. by S.C. Singh, H. Zeng, C. Guo and W. Cai, (Wiley-VCH Verlag, Weinheim, 2012) pp. 255–316.
[24] C. B. Arnold, P. Serra and A. Pique: MRS Bull., 32, (2007) 23.
[25] P. Serra, M. Duocastella, J. M. Fernández-Pradas and J. L. Morenza: "Cell and Organ Printing" ed. by R.B. Ringeisen, J.B. Spargo and K.P. Wu, (Springer Netherlands, Dordrecht, 2010) pp. 53–8
[26] A. Pique and H. Kim: J. Laser Micro/Nanoengin., 9, (2014) 192.
[27] A. Pique, R. C. Auyeung, H. Kim, K. M. Metkus and S. A. Mathews: J. Laser Micro/Nanoengin., 3, (2008) 163.
[28] J. Bohandy, B. F. Kim, F. J. Adrian and A. N. Jette: J. Appl. Phys., 63, (1988) 1158.
[29] J. A. Grant-Jacob, B. Mills, M. Feinaeugle, C. L. Sones, G. Oosterhuis, M. B. Hoppenbrouwers and R. W. Eason: Opt. Mater. Express, 3, (2013) 747.
[30] C. W. Visser, R. Pohl, C. Sun, G. W. Roemer, B. H. in 't Veld and D. Lohse: Adv. Mater., 27, (2015) 4087.
[31] Q. Li, A. P. Alloncle, D. Grojo and P. Delaporte: Opt Express, 25, (2017) 24164.
[32] M. Zenou, A. Sa'ar and Z. Kotler: Sci. Rep., 5, (2015) 17265.
[33] Y. Berg, S. Winter, Z. Kotler andY. Shacham-Diamand: J. Laser Micro/Nanoengin., 13, (2018) 131.
[34] S. Winter, M. Zenou and Z. Kotler: J. Phys. Appl. Phys., 49, (2016) 165310.
[35] J. Schrauben: Manuscript in Preparation (2018).
[36] D Du, X. Liu, G. Korn, J. Squier and G. Mourou: Appl. Phys. Lett., 64, (1994) 3071.
[37] K. Sugioka and Y. Cheng: Lab Chip, 12, (2012) 3576.
[38] S. Karimelahi, L. Abolghasemi and P. R. Herman: Appl. Phys. A, 114, (2014) 91.
[39] A. Otto, H. Koch, R. Gomez Vazquez, Z. Lin and B. Hainsey: Phys. Procedia, 56, (2014) 1315.
[40] D. Finn, Z. Lin, J. Kleinert, M. Darwin and H. Zhang: J. Laser Appl., 27, (2015) 032004.
[41] A. Otto, H. Koch, K. Leitz and M. Schmidt: Phys. Procedia, 12-A, (2011) 11.
[42] A. Otto, H. Koch and R. Gomez Vazquez: Phys. Procedia, 39, (2012) 843.
[43] D. W. Bäuerle: "Laser Processing and Chemistry" (Springer-Verlag, Berlin, 2011).

(Received: September 26, 2018, Accepted: January 27, 2019)